Temperature-dependent XAFS parameters of crystalline platinum within a classical anharmonic correlated Einstein approach

Vu Quang Tho[1], Nguyen To Nu[2], Nguyen Thi Minh Thuy[3], Tong Sy Tien[3*]

[1]Faculty of Physics, Tan Trao University, Trung Mon 16, Minh Xuan, Tuyen Quang, Vietnam;
[2]Department of Physics, Hanoi Pedagogical University 2, 32 Nguyen Van Linh, Xuan Hoa, Phu Tho, Vietnam;
[3]Faculty of Fundamental Sciences, University of Fire Prevention and Fighting, 234 Khuat Duy Tien, Dai Mo, Hanoi, Vietnam.
[*]Corresponding author: tongsytien@yahoo.com
Received 11 Mar. 2026; Revised 18 May 2026; Accepted 15 Jun. 2026; Published 25 Jun. 2026.
DOI: https://doi.org/10.54939/1859-1043.j.mst.112.2026.157-166

ABSTRACT

Temperature-dependent thermodynamic XAFS parameters of crystalline platinum (Pt) are investigated using a classical anharmonic correlated-Einstein approach that accounts for thermal disorder. The method is based on an anharmonic effective potential and classical statistical theory, from which effective force constants, Einstein temperature, and Einstein frequency are consistently obtained. Anharmonic lattice vibrations are treated using a fourth-order cumulant expansion, yielding analytical expressions for the first four XAFS cumulants over the temperature range 0–800 K. The results are consistent with experimental data and quantum anharmonic-correlated Einstein calculations in the intermediate- and high-temperature regimes. Higher-order cumulants play a dominant role in describing anharmonicity and non-Gaussian features of the atomic distribution, remaining valid over a wider temperature range, including part of the region below the Einstein temperature. The present approach therefore provides a consistent and efficient description of temperature-dependent thermodynamic XAFS parameters of Pt.

Keywords: XAFS cumulant; Classical statistical approach; Temperature dependence; Crystalline platinum

1. INTRODUCTION

Thermodynamic properties of crystalline materials are governed by lattice vibrations, which evolve with temperature due to anharmonicity in the interatomic potential [1]. At elevated temperatures, phonon–phonon interactions induce deviations from harmonic behavior, leading to non-Gaussian atomic distributions reflected in the radial distribution function [2]. Within the XAFS framework, these effects are encoded in the oscillatory absorption signal through the distribution of interatomic distances [3]. The cumulant expansion formalism describes this behavior via temperature-dependent cumulants, with lower-order terms representing quasi-harmonic contributions and higher-order terms accounting for anharmonicity [4]. Therefore, accurate XAFS analysis requires explicit treatment of anharmonic effects beyond the Gaussian approximation [5].

Anharmonic XAFS oscillations are strongly influenced by thermal disorder arising from lattice vibrations, resulting in phase shifts and amplitude modulation of the signal [6]. As noted by Eisenberger & Brown, neglecting these effects leads to significant errors in the extracted thermodynamic parameters [7]. To account for anharmonic deviations from Gaussian behavior, Bunker introduced the cumulant expansion approach [8]. Consequently, accurate XAFS analysis requires theoretical models that explicitly incorporate anharmonic effects [9]. Within the plane-wave and single-scattering approximations, the XAFS signal can be expressed in terms of the leading cumulants of the radial distribution function as follows [10]:

$$\chi(k) = F(k)\frac{e^{-2R/\lambda(k)}}{kR^2} Im\left\{ e^{i\Phi(k)} \exp\left[2ikR + \sum_n \frac{(2ik)^n}{n!}\sigma^{(n)} \right] \right\} \quad (1)$$

where $R = \langle r \rangle$ with $\langle r \rangle$ represents the instantaneous bond length between backscattering and absorbing atoms, k is the photoelectron wavenumber, $\delta(k)$ represents the net phase shift, $\lambda(k)$ is the mean free path of the photoelectron, $F(k)$ corresponds to the atomic backscattering amplitude, and $\sigma^{(n)}$ are the **n**th cumulant.

Platinum (Pt) is a chemically stable crystalline metal with well-defined lattice properties, making it a suitable system for investigating temperature-dependent lattice dynamics and thermal disorder [11]. Its relatively large atomic mass and well-characterized phonon spectrum provide favorable conditions for analyzing anharmonic vibrational effects within the XAFS framework [12]. In particular, Pt has been extensively studied as a reference system in XAFS spectroscopy, where thermodynamic parameters can be extracted from temperature-dependent measurements [13-15]. Experimental XAFS cumulants of Pt in the temperature range from 30 to 800 K were reported by Okube & Yoshiasa using synchrotron radiation at the Photon Factory (KEK-PF), Japan [16].

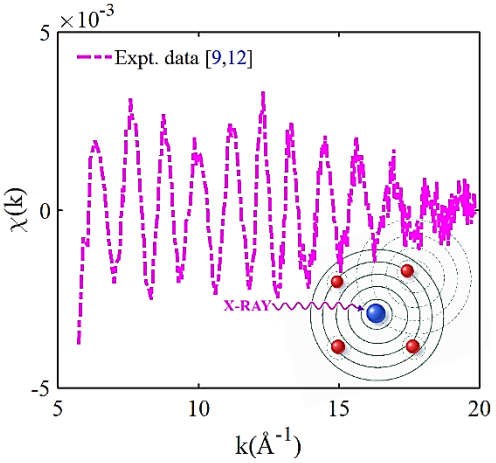

Figure 1. *The XAFS signal of Pt at room temperature obtained from the experimental data [9, 12].*

The experimental XAFS signal of Pt at room temperature is shown in Figure 1, illustrating the characteristic oscillatory behavior $\chi(k)$ arising from photoelectron backscattering in the crystal lattice. Consequently, the temperature-dependent evolution of XAFS spectra must be explicitly taken into account in the analysis.

Among available approaches, the classical anharmonic correlated Einstein (CACE) model provides a tractable framework for describing anharmonic lattice vibrations in crystalline metals [17]. Its advantage lies in explicit analytical expressions for XAFS cumulants, enabling direct evaluation of thermodynamic parameters and comparison with experiment [18]. Although its classical nature neglects quantum zero-point (ZP) vibrations, limiting its validity at low temperatures, this approach remains effective at intermediate and high temperatures, where thermal vibrations are predominantly classical [19]. Therefore, it is well-suited for analyzing thermodynamic XAFS parameters of Pt within the experimentally accessible temperature range.

2. FORMULAS AND CALCULATIONS

The pair interaction (PI) potential of metals is commonly described by the Morse potential, which captures anharmonic interatomic bonding [20]. For analytical treatment, it is convenient to expand this potential around its equilibrium position up to the fourth order, allowing both harmonic and anharmonic contributions to be explicitly incorporated as [18].

$$V(x) = D\left(e^{-2\alpha x} - 2e^{-\alpha x}\right) \approx -D + D\alpha^2 x^2 - D\alpha^3 x^3 + 7D\alpha^4 x^4 / 12,\ x = r - r_0 \qquad (2)$$

where α characterizes the PI potential width, D denotes the dissociation energy, x is the instantaneous displacement, and r_0 and r represent the equilibrium and instantaneous bond lengths, respectively.

Normally, one needs to determine the anharmonic effective (AE) potential from the atomic interaction potential of single-bond (SB) pairs in the crystal lattice, which is then used to identify the system's thermodynamic parameters [21]. The AE potential in the relative vibrations of backscattering (B) and absorbing (A) atoms can be calculated using the PI potential [22]:

$$V_{eff} = V(x) + \sum_{i=A,B} \sum_{j \neq A,B} V\left(\varepsilon_i x \hat{R}_{AB} \hat{R}_{ij}\right), \qquad \varepsilon_i = \frac{\mu}{m_i} \tag{3}$$

where $\mu = m_A m_B / \left(m_A + m_B\right)$ is the reduced mass of a single bond pair with atomic masses m_A and m_B, m_i is the mass of the ith atom, $\hat{R}$ is the bond unit vector, sum i is the over backscattering and absorbing atoms, and the sum j is over all their nearest neighbors.

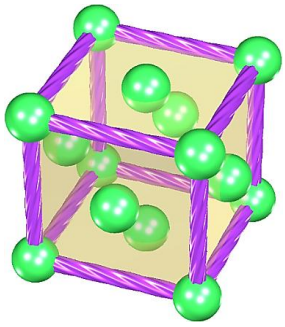

Figure 2. *The structural model of Pt.*

The crystalline structure of Pt in a face-centered cubic (FCC) lattice is shown in Figure 2, consisting of identical atoms arranged so that eight atoms occupy the cube corners and six atoms occupy the face centers [23]. In a monoatomic crystal, all atoms have the same mass m, which simplifies the description of lattice vibrations [1]. After using structural characteristics, the AE potential of Pt is obtained by Equation (3) and is presented as

$$V_{eff}(x) = V(x) + 4V(0) + 2V\left(-x/2\right) + 8V\left(x/4\right) + 8V\left(-x/4\right) \tag{4}$$

The result of AE potential can be obtained from Equation (4) using the Morse potential in Equation (2). After ignoring the constant contribution in the approximate expansion to the 4th order, the AE potential can be presented in the form:

$$V_{eff}(x) = k_{eff} x^2 / 2 - k_{3an} x^3 + k_{4an} x^4 \tag{5}$$

where k_{eff} is an effective force constant, k_{3an} and k_{4an} are the anharmonic force constants, which are not temperature-dependent and are written as

$$k_{eff} = 5D\alpha^2, \quad k_{3an} = 5D\alpha^3 / 4, \quad k_{4an} = 133D\alpha^4 / 192 \tag{6}$$

The CACE model [24], developed from the correlated Einstein (CE) model [25] within classical statistical theory [19] and based on the AE potential [22], provides explicit temperature-dependent expressions for XAFS cumulants. Its applicability has been established for anharmonic XAFS analysis of metals over a wide temperature range up to near the melting point [17, 18].

In this model, thermal vibrations in crystalline solids are described in terms of phonons and are characterized by the Einstein frequency ω_E and temperature θ_E, which are determined from the effective force constant [21], as given below

$$\omega_E = \sqrt{\frac{k_{eff}}{\mu}} = \alpha\sqrt{\frac{10D}{M}}, \quad \theta_E = \frac{\hbar\omega_E}{k_B} = \frac{\hbar\alpha}{k_B}\sqrt{\frac{10D}{M}} \tag{7}$$

where and $\hbar$ and k_B are the reduced Planck and Boltzmann constants, respectively.

The temperature-dependent XAFS cumulants are determined from the moments of the radial pair distribution (RPD) function [26]. In the cumulant expansion formalism, the first four cumulants are expressed in terms of the moments $\langle x^n \rangle$ [27]. Using the anharmonic effective potential in Equation (5), these moments can be evaluated within classical statistical theory by treating anharmonicity as a small perturbation up to third order based on the thermal averages defined as [19].

$$\langle x^n \rangle = \frac{\int_{-\infty}^{\infty} x^n \exp\left[-\frac{V_{eff}(x)}{k_B T}\right] dx}{\int_{-\infty}^{\infty} \exp\left[-\frac{V_{eff}(x)}{k_B T}\right] dx} \approx \frac{\int_{-\infty}^{\infty} x^n \exp\left[\frac{-k_{eff}x^2}{2k_B T}\right]\left[\sum_{n=0}^{3}\frac{1}{n!}\left(\frac{k_{3an}x^3 - k_{4an}x^4}{k_B T}\right)^n\right] dx}{\left(\frac{2\pi k_B T}{k_{eff}}\right)^{1/2}\left[1 + \frac{3(k_B T)}{k_{eff}^2}\left(\frac{5k_{3an}^2}{2k_{eff}} - k_{4an}\right)\right]} \tag{8}$$

The force constants obtained from Equation (6) are substituted into Equation (8) to evaluate the moments $\langle x^n \rangle$ for $n = 1 \div 4$. The first four XAFS cumulants are then determined from these moments via their definitions within the cumulant expansion formalism [10, 18], yielding explicit analytical expressions as functions of temperature, given as follows:

$$\sigma^{(1)} = \langle r \rangle - r_0 = \langle x \rangle \simeq \frac{3k_B T}{20D\alpha}\left(1 - \frac{389k_B T}{1200D}\right) \tag{9}$$

$$\sigma^{(2)} = \left\langle \left(r - \langle r \rangle\right)^2 \right\rangle = \langle x^2 \rangle - \langle x \rangle^2 \simeq \frac{k_B T}{5D\alpha^2}\left(1 + \frac{47k_B T}{400D}\right) \tag{10}$$

$$\sigma^{(3)} = \left\langle \left(r - \langle r \rangle\right)^3 \right\rangle = \langle x^3 \rangle - 3\langle x^2 \rangle\langle x \rangle + 2\langle x \rangle^3 \simeq \frac{3(k_B T)^2}{50D^2\alpha^3}\left(1 - \frac{211k_B T}{400D}\right) \tag{11}$$

$$\begin{aligned}\sigma^{(4)} &= \left\langle \left(r - \langle r \rangle\right)^4 \right\rangle - 3\left[\sigma^{(2)}\right]^2 = \langle x^4 \rangle + 12\langle x^2 \rangle\langle x \rangle^2 - 3\langle x^2 \rangle^2 - 4\langle x^3 \rangle\langle x \rangle - 6\langle x \rangle^4 \\ &\simeq \frac{137(k_B T)^3}{5000D^3\alpha^4}\left(1 + \frac{50649k_B T}{54800D}\right)\end{aligned} \tag{12}$$

In the regime $k_B T/D << 1$, anharmonic contributions remain small, and only the lowest-order terms in the expansion need to be retained [17, 19]. Under this condition, the temperature-dependent XAFS cumulants can be approximated as follows:

The first cumulant characterizes the net thermal expansion (NTE) [8, 26] and is written as

$$\sigma^{(1)} \approx \frac{3k_B T}{20D\alpha} = \frac{3\alpha}{4}\sigma^2 \tag{13}$$

The second cumulant characterizes the mean-square relative displacement (MSRD) [8, 26] and is written as

$$\sigma^{(2)} \approx \frac{k_B T}{5D\alpha^2} \equiv \sigma^2 \tag{14}$$

The third cumulant characterizes the mean cubic relative displacement (MCRD) [8, 28] and is written as

$$\sigma^{(3)} \approx \frac{3\left(k_B T\right)^2}{50 D^2 \alpha^3} = \frac{3\alpha}{2}\left(\sigma^2\right)^2 \tag{15}$$

The fourth cumulant characterizes the non-Gaussian distribution function (NGDF) [8, 28] and is written as

$$\sigma^{(4)} \approx \frac{137\left(k_B T\right)^3}{5000 D^3 \alpha^4} = \frac{137\alpha^2}{40}\left(\sigma^2\right)^3 \tag{16}$$

Thus, within the CACE framework, the cumulants are obtained in explicit analytical forms as functions of temperature. In the leading-order approximation, the first, second, third, and fourth cumulants exhibit characteristic temperature dependences proportional to T, T, T^2, and T^3, respectively. Moreover, the higher-order cumulants can be expressed in terms of the second cumulant σ^2, indicating that the fundamental vibrational amplitude systematically governs anharmonic contributions.

3. RESULTS AND DISCUSSIONS

In this section, numerical results for Pt are obtained using the present CACE model based on the analytical expressions in Sec. 2 and the corresponding physical parameters. The atomic mass of Pt is taken as M = 195.084 u [29], while the Morse potential parameters are $D = 0.5896$ eV and $\alpha = 1.3412$ Å^{-1}, determined from experimental XAFS data using an effective method for metals [16]. The results are compared with the quantum anharmonic correlated Einstein (QACE) results [15], and with experimental data measured by Pirog & Nedoseikina at the synchrotron radiation Siberian center (SRSC, Russia) [30] and by Okube and Yoshiasa at BL10B of KEK-PF (Japan) [16]. Calculations are performed over the temperature range of 0–800 K. The model's performance is evaluated by examining the temperature dependence of XAFS parameters for Pt under thermal disorder. The corresponding results and discussion are presented below.

The local force constants k_{eff}, k_{3an}, and k_{4an}, together with the Einstein frequency ω_E and temperature θ_E, characterize the strength of atomic thermal vibrations. Using the present CACE model, these parameters are obtained from Equations (6) and (7) as $k_{eff} \simeq 5.30$ eVÅ^{-2}, $k_{3an} \simeq 1.78$ eVÅ^{-3}, $k_{4an} \simeq 1.32$ eVÅ^{-4}, $\omega_E \simeq 2.29\times10^{13}$ Hz, and $\theta_E \simeq 175$ K. Experimental values derived from XAFS measurements at SRSC (Russia) $k_{eff} \simeq 5.0 \pm 0.2$ eVÅ^{-2}, $k_{3an} \simeq 2.0 \pm 0.1$ eVÅ^{-3}, $\omega_E \simeq \left(2.22 \pm 0.05\right)\times10^{13}$ Hz, and $\theta_E \simeq \left(170 \pm 4\right)$ K [30]. The Einstein frequency and temperature are obtained from the effective force constant. The comparison shows good agreement within uncertainties, particularly for ω_E and θ_E.

The AE potential $V_{eff}\left(x\right)$ and its components are in the range from −0.30 Å to 0.30 Å, calculated from Equation (5) using the corresponding force constants above, which are shown in Fig. 3. The AE potential $V_{eff}\left(x\right)$ is decomposed as $V_{eff}\left(x\right) = V_{ha}\left(x\right) + V_{an}\left(x\right)$, where $V_{ha}\left(x\right) = k_{eff}x^2$ is the harmonic contribution and $V_{an}\left(x\right) = -k_{3an}x^3 + k_{4an}x^4$ describes anharmonic contributions. The second-order component $(k_{eff}x^2)$ defines the harmonic restoring interaction and the curvature near equilibrium $\left(x = 0\right)$. The third-order component $(-k_{3an}x^3)$ introduces intrinsic asymmetry in the potential. The fourth-order component $(k_{4an}x^3)$ ensures stability and boundedness at larger displacements.

As a result, the total components deviate progressively from a purely quadratic form with increasing |*x*|, exhibiting a pronounced asymmetry between negative and positive displacements.

This asymmetry originates primarily from the third-order component, which is positive for $x<0$ negative for $x>0$, while the even-order components remain strictly positive. For example, at $x=-0.20$ Å and $x=0.20$ Å the harmonic component remains constant at $V_{ha}=0.106$ eV, while the anharmonic components change sign, with $V_{an}=0.016$ eV at $x=-0.20$ Å and $V_{an}=-0.012$ eV at $x=0.20$ Å. Accordingly, the total components are $V_{eff}=0.122$ eV and 0.094 eV, respectively, in good agreement with the experimental values $V_{eff}=0.116\pm0.005$ eV and $V_{eff}=0.084\pm0.005$ eV reported by Pirog and Nedoseikina [30]. This confirms that the present CACE model captures the essential anharmonicity of the Pt interatomic interaction, as evidenced by the sign reversal of $V_{an}(x)$, which reflects the intrinsic asymmetry of the AE potential.

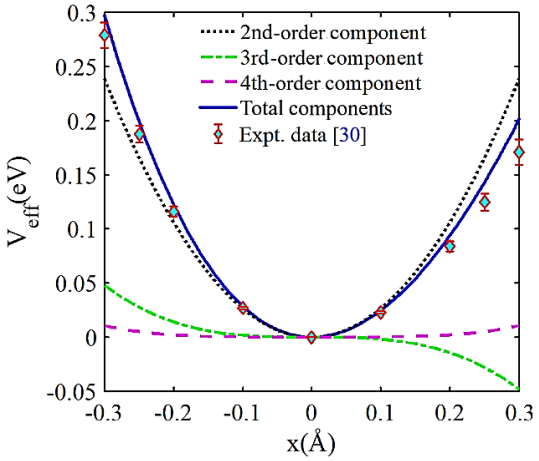

Figure 3. *The position-dependent AE potential of Pt obtained from the present CACE model, together with its 2nd-, 3rd-, and 4th-order components in comparison with experimental data [30].*

The temperature dependence of the first four XAFS cumulants $\sigma^{(n)}(T)$ $(n=1\div4)$ of Pt in the range 0–800 K is shown in Figure 4. The present CACE results are calculated from Equation (13) to Equation (16), while the QACE results are taken from Reference [15]. The experimental data with error bars were measured by Okube and Yoshiasa at beamline BL10B of KEK-PF (Tsukuba, Japan) [16], and are used for direct comparison. For the first and second (low-order) cumulants, the present CACE results agree with both QACE predictions [15] and experimental data at temperatures $T\geq\theta_E$. In this regime, thermal vibrations are well described by classical statistics. However, in the low-temperature (LT) regime $T<<\theta_E$, the present CACE model yields vanishing values as $T\to0$, reflecting the absence of quantum ZP motion [4]. In contrast, the QACE model [15] captures finite values due to quantum lattice effects. For the third and fourth (high-order) cumulants, which characterize anharmonicity and non-Gaussian behavior [28], the present CACE results remain consistent with QACE predictions [15] and experimental data [16] over a broader temperature range, extending partially into the LT regime $T<\theta_E$.

This indicates that higher-order cumulants are less sensitive to quantum effects at low temperatures, while anharmonic contributions dominate at elevated temperatures. Physically, the low-order cumulants are governed mainly by harmonic vibrational amplitudes and are therefore more sensitive to quantum ZP motion in the LT regime. In contrast, the high-order cumulants primarily reflect anharmonic asymmetry and non-Gaussian features of the atomic distribution, whose relative quantum corrections are weaker. As a result, the present CACE model remains reasonably consistent with QACE predictions and experiments over a broader temperature range,

extending partially below the Einstein temperature. Overall, the present CACE model provides a reliable description of temperature-dependent XAFS cumulants of Pt for regime $T \geq \theta_E$.

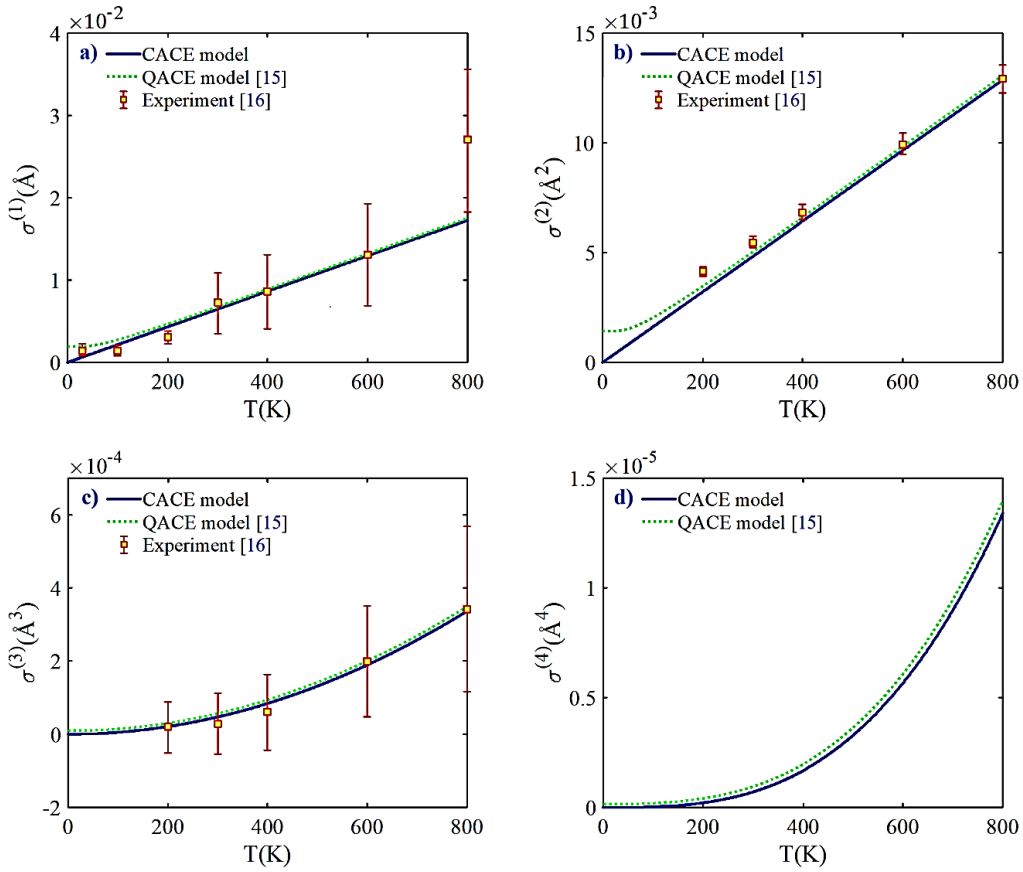

Figure 4. *The temperature dependence of the first four XAFS cumulants of Pt obtained from the present CACE model in comparison with QACE results [15] and experimental data [16].*

The temperature-dependent values of the first four XAFS cumulants of Pt obtained from the present CACE model, QACE model [15], and experimental data [16] are listed in Table 1. A direct comparison indicates that the present CACE results progressively converge to the QACE predictions [15] and the experimental values of Okube and Yoshiasa [16] as the temperature increases, whereas significant deviations remain at low temperatures. For the low-order cumulants, the discrepancies are more evident at low temperatures, whereas the agreement improves progressively at higher temperatures. A noticeable deviation is observed for the first cumulant at 800 K, where anharmonic thermal expansion becomes increasingly pronounced. Nevertheless, the calculated value remains close to the experimental uncertainty range, indicating that the overall temperature-dependent behavior is still reasonably reproduced by the CACE model. The discrepancy observed in the first cumulant at 800 K is likely due to enhanced anharmonic thermal expansion at high temperature, where classical approximations become less accurate. However, the calculated result still lies close to the experimental uncertainty range, preserving the overall consistency of the temperature-dependent behavior. In contrast, the higher-order cumulants exhibit closer agreement over a broader temperature range. This indicates that higher-order cumulants are less affected by the limitations of the classical treatment [19]. Universal, the numerical data demonstrate that the present CACE model captures the main temperature-dependent trends of XAFS cumulants and provides consistent values with reference results in the temperature range where thermal vibrations dominate.

Thus, the first four XAFS cumulants of Pt obtained from the present CACE model are consistent with QACE and experimental results at temperatures $T \geq \theta_E$, where classical statistics is applicable. These cumulants describe the thermal-vibrational contributions governing the temperature dependence of the XAFS signal, with anharmonic effects becoming increasingly significant above about room temperature. Consequently, the present CACE model provides a reliable description of temperature-dependent XAFS cumulants of Pt in medium and high temperature regimes, particularly for higher-order cumulants associated with anharmonic lattice dynamics.

Table 1. *The XAFS cumulants of Pt obtained from the present CACE and QACE modes and experiment.*

Cumulant	T (K)	CACE model [a]	QACE model [b]	Experiment [c]
$\sigma^{(1)}$ ($\times 10^{-2}$ Å)	30	0.06	0.19	0.14 ± 0.08
	100	0.22	0.27	0.14 ± 0.07
	200	0.42	0.46	0.31 ± 0.08
	300	0.64	0.67	0.74 ± 0.38
	400	0.86	0.89	0.86 ± 0.45
	600	1.28	1.32	1.31 ± 0.62
	800	1.71	1.75	2.71 ± 0.86
$\sigma^{(2)}$ ($\times 10^{-2}$ Å^2)	30	0.05	0.14	-
	100	0.16	0.20	0.30 ± 0.02
	200	0.32	0.35	0.42 ± 0.02
	300	0.48	0.51	0.54 ± 0.03
	400	0.64	0.66	0.68 ± 0.04
	600	0.96	0.98	0.99 ± 0.05
	800	1.29	1.31	1.29 ± 0.06
$\sigma^{(3)}$ ($\times 10^{-4}$ Å^3)	30	0.01	0.02	-
	100	0.05	0.09	-
	200	0.21	0.25	0.23 ± 0.67
	300	0.48	0.52	0.28 ± 0.84
	400	0.85	0.89	0.60 ± 1.02
	600	1.90	1.95	1.98 ± 1.51
	800	3.38	3.43	3.41 ± 2.26
$\sigma^{(4)}$ ($\times 10^{-6}$ Å^4)	30	0.00	0.03	-
	100	0.03	0.07	-
	200	0.21	0.29	-
	300	0.72	0.84	-
	400	1.69	1.85	-
	600	5.71	5.95	-
	800	13.53	13.85	-

[a] *Values obtained from the present CACE model.*
[c] *Values calculated using the QACE model [15].*
[d] *Experimental values taken by Okube and Yoshiasa [16].*

4. CONCLUSIONS

In this work, the temperature-dependent thermodynamic XAFS parameters of Pt have been investigated within the CACE framework, accounting for thermal disorder. The first four XAFS cumulants are derived in explicit analytical forms, enabling a consistent description of both harmonic and anharmonic lattice vibrations. The results show that the present CACE model

reproduces the temperature dependence of the cumulants in a consistent manner with the QACE calculation and experimental data in the intermediate and high-temperature regimes, extending to temperatures close to the melting point. The deviations observed at low temperatures arise from the model's classical nature, which does not include quantum ZP vibrations.

The analysis indicates that high-order cumulants remain well described over a broader temperature range, including part of the regime $T < \theta_E$, while the low-order cumulants require a regime $T \geq \theta_E$ for accurate agreement. These results highlight the role of anharmonic effects and non-Gaussian features of atomic distributions at elevated temperatures. Owing to its analytical simplicity and physical transparency, the model provides an efficient framework for interpreting temperature-dependent XAFS data and can be extended to other crystalline metals over a broad temperature range, up to temperatures approaching the melting point.

Acknowledgments: *This research is funded by Tan Trao University under grant number 2025.1.16.*

REFERENCES

[1]. S. H. Simon, "*The Oxford Solid State Basics*," 1st ed., Oxford University Press, Oxford, (2013).
[2]. G. Bunker, "*Introduction to XAFS: A Practical Guide to X-ray Absorption Fine Structure Spectroscopy*," Cambridge University Press, Cambridge, (2010).
[3]. M. Newville, "*Fundamentals of XAFS*," Rev. Mineral. Geochem., vol. 78, no. 1, pp. 33–74, (2014).
[4]. T. Yokoyama, S. Chaveanghong, "*Anharmonicity in elastic constants and extended x-ray-absorption fine structure cumulants*," Phys. Rev. Mater., vol. 3, art. 033607, (2019).
[5]. L. Tröger, T. Yokoyama, D. Arvanitis, T. Lederer, M. Tischer, K. Baberschke, "*Determination of bond lengths, atomic mean-square relative displacements, and local thermal expansion by means of soft-x-ray photoabsorption*," Phys. Rev. B, vol. 49, no. 2, pp. 888–903, (1994).
[6]. G. Dalba, P. Fornasini, M. Grazioli, F. Rocca, "*Local disorder in crystalline and amorphous germanium*," Phys. Rev. B, vol. 52, no. 15, pp. 11034–11043, (1995).
[7]. P. Eisenberger, G. S. Brown, "*The study of disordered systems by EXAFS: Limitations*," Solid State Commun., vol. 29, no. 6, pp. 481–484, (1979).
[8]. G. Bunker, "*Application of the ratio method of EXAFS analysis to disordered systems*," Nucl. Instrum. Methods, vol. 207, pp. 437–444, (1983).
[9]. J. J. Rehr, R. C. Albers, "*Theoretical approaches to X-ray absorption fine structure*," Rev. Mod. Phys., vol. 72, no. 3, pp. 621–654, (2000).
[10]. E. D. Crozier, J. J. Rehr, R. Ingalls, "*Amorphous and liquid systems*," in *X-ray Absorption: Principles, Applications, Techniques of EXAFS, SEXAFS, XANES*, D. C. Koningsberger, R. Prins (Eds.), Wiley, New York, (1988).
[11]. L. Wood, "*The Elements: Platinum*," Cavendish Square Publishing LLC, New York, (2004).
[12]. Y. Nishihata, O. Kamishima, Y. Kubozono, H. Maeda, S. Emura, "*XAFS in the high-energy regime*," J. Synchrotron Radiat., vol. 5, pp. 1007–1009, (1998).
[13]. N. H. Thao, N. T. M. Thuy, D. S. Lan, L. V. Hoang, T. S. Tien, "*Debye-Waller factor of Pt in X-ray absorption fine structure analyzed using classical anharmonic correlated Einstein model*," Commun. Phys., vol. 35, art. 22594, (2025).
[14]. N. B. Duc, V. Q. Tho, T. S. Tien, D. Q. Khoa, H. K. Hieu, "*Pressure and temperature dependence of EXAFS Debye-Waller factor of platinum*," Radiat. Phys. Chem., vol. 149, pp. 61–64, (2018).
[15]. L. D. Manh, N. T. M. Thuy, N. B. Trung, N. C. Toan, N. T. B. Son, T. S. Tien, "*Effect of Thermal Disorder on Thermodynamic Parameters of Platinum in Anharmonic EXAFS Theory*," Phys. Status Solidi B, vol. 262, art. 202400604, (2025).
[16]. M. Okube, A. Yoshiasa, "*Anharmonic effective pair potentials of group VIII and Ib fcc metals*," J. Synchrotron Radiat., vol. 8, pp. 937–939, (2001).
[17]. N. V. Hung, T. S. Tien, N. B. Duc, D. Q. Vuong, "*High-order expanded XAFS Debye-Waller factors of HCP crystals based on classical anharmonic correlated Einstein model*," Mod. Phys. Lett. B, vol. 28, no. 21, art. 1450174, (2014).
[18]. T. S. Tien, "*Analysis of EXAFS oscillation of FCC crystals using classical anharmonic correlated Einstein model*," Radiat. Phys. Chem., vol. 186, art. 109504, (2021).

[19]. E. A. Stern, P. Livins, Z. Zhang, "*Thermal vibration and melting from a local perspective*," Phys. Rev. B, vol. 43, pp. 8850–8860, (1991).
[20]. L. A. Girifalco, V. G. Weizer, "*Application of the Morse potential function to cubic metals*," Phys. Rev., vol. 114, no. 3, pp. 687–690, (1959).
[21]. N. B. Duc, N. V. Hung, H. D. Khoa, D. Q. Vuong, T. S. Tien, "*Thermodynamic properties and anharmonic effects in XAFS based on anharmonic correlated Debye model*," Adv. Mater. Sci. Eng., vol. 2018, art. 3263170, (2018).
[22]. N. V. Hung, J. J. Rehr, "*Anharmonic correlated Einstein-model Debye-Waller factors*," Phys. Rev. B, vol. 56, no. 1, pp. 43–46, (1997).
[23]. C. Kittel, "*Introduction to Solid State Physics*," 8th ed., Wiley, New York, (2004).
[24]. T. S. Tien et al., "*High-order EXAFS cumulants of diamond crystals based on a classical anharmonic correlated Einstein model*," J. Phys. Chem. Solids, vol. 134, pp. 307–312, (2019).
[25]. E. Sevillano, H. Meuth, J. J. Rehr, "*Extended X-ray absorption fine structure Debye-Waller factors. I. Monatomic crystals*," Phys. Rev. B, vol. 20, pp. 4908–4911, (1979).
[26]. J. J. Rehr et al., "*EXAFS: theory and approaches*," Int. Tables Crystallogr., pp. 71–79, (2024).
[27]. T. Yokoyama, K. Kobayashi, T. Ohta, A. Ugawa, "*Anharmonic interatomic potentials of diatomic and linear triatomic molecules studied by extended X-ray absorption fine structure*," Phys. Rev. B, vol. 53, no. 10, pp. 6111–6122, (1996).
[28]. J. M. Tranquada, R. Ingalls, "*Extended x-ray-absorption fine-structure study of anharmonicity in CuBr*," Phys. Rev. B, vol. 28, no. 6, pp. 3520–3528, (1983).
[29]. N. W. Ashcroft, N. D. Mermin, "*Solid State Physics*," Holt, Rinehart & Winston, New York, (1976).
[30]. I. V. Pirog, T. I. Nedoseikina, "*Study of effective pair potentials in cubic metals*," Physica B, vol. 334, pp. 123–129, (2003).

TÓM TẮT

Các tham số XAFS phụ thuộc nhiệt độ của tinh thể bạch kim trong khuôn khổ mô hình Einstein tương quan phi điều hòa cổ điển

Các tham số nhiệt động XAFS phụ thuộc nhiệt độ của tinh thể bạch kim (Pt) được khảo sát trong khuôn khổ mô hình Einstein tương quan phi điều hòa cổ điển dưới ảnh hưởng của rối loạn nhiệt. Phương pháp dựa trên thế hiệu dụng phi điều hòa và lý thuyết thống kê cổ điển, từ đó các hằng số lực hiệu dụng, nhiệt độ Einstein và tần số Einstein được xác định một cách nhất quán. Dao động mạng phi điều hòa được mô tả bằng khai triển cumulant đến bậc bốn, cho phép thu được các biểu thức giải tích cho bốn cumulant đầu tiên của XAFS trong khoảng nhiệt độ 0–800 K. Kết quả cho thấy sự phù hợp với dữ liệu thực nghiệm và các tính toán theo mô hình Einstein tương quan phi điều hòa lượng tử trong miền nhiệt độ trung bình và cao. Các cumulant bậc cao đóng vai trò quyết định trong việc mô tả tính phi điều hòa và các đặc trưng phi Gauss của phân bố nguyên tử, đồng thời vẫn còn hiệu lực trong một khoảng nhiệt độ rộng hơn, bao gồm cả một phần miền dưới nhiệt độ Einstein. Do đó, phương pháp này cung cấp một mô tả nhất quán và hiệu quả đối với các tham số nhiệt động XAFS phụ thuộc nhiệt độ của Pt.

Từ khoá: Cumulant XAFS; Phương pháp thống kê cổ điển; Sự phụ thuộc nhiệt độ; Tinh thể bạch kim.